Kitaev honeycomb models in magnetic fields: Dynamical response and dual models

David A. S. Kaib,* Stephen M. Winter, and Roser Valentí
Institut für Theoretische Physik, Goethe-Universität Frankfurt, Max-von-Laue-Strasse 1, 60438 Frankfurt am Main, Germany

(Received 17 April 2019; revised manuscript received 16 August 2019; published 30 October 2019)

Motivated by recent reports of a field-induced *intermediate phase* (IP) in the antiferromagnetic honeycomb Kitaev model that may be a spin liquid whose nature is distinct from the Kitaev $\mathbb{Z}_2$ phase, we present a detailed numerical study on the nature and dynamical response (such as dynamical spin-structure factors and resonant inelastic x-ray scattering intensities) of this field-induced IP and neighboring phases in a family of Kitaev-based models related by hidden symmetries and duality transformations. We further show that the same field-induced IP can appear in models relevant for α-$RuCl_3$, which exhibit a ferromagnetic Kitaev coupling and additional interactions. In α-$RuCl_3$, the IP represents a new phase, that is likely independent from the putative field-induced (spin-liquid) phase recently reported from thermal Hall conductivity measurements.

DOI: 10.1103/PhysRevB.100.144445

I. INTRODUCTION

In magnets with strongly frustrated interactions, quantum spin liquids can arise as exotic phases of matter that feature long-range entanglement and fractionalized excitations. A prime example is the exactly solvable Kitaev model on the honeycomb lattice [1], which hosts a quantum spin liquid ground state of itinerant Majorana fermions that couple to a static $\mathbb{Z}_2$ gauge field.

Material realizations of the Kitaev model have been heavily sought after, and a mechanism [2] relying on an intricate interplay of strong electronic correlations, crystal field splitting, and spin-orbit coupling has brought candidate materials such as Na_2IrO_3, various polymorphs of Li_2IrO_3, and α-$RuCl_3$ to the forefront of research. However, these materials all display magnetic order at low temperatures, which is a result of additional magnetic couplings extending beyond the pure Kitaev coupling. With the goal of unravelling potential residual fractionalized excitations reminiscent of the pure Kitaev model in materials, there have been various routes to suppress the magnetic order, including the application of pressure [3–6], finite temperatures [7–9] or a magnetic field [10–21]. For the latter case, a putative field-induced phase [14–16,18,20] in α-$RuCl_3$, that lacks magnetic order, is under strong scrutiny. Here, a half-integer quantized thermal Hall conductivity was recently reported [20] for fields tilted by 30° and 45° out of the honeycomb plane. Such measurements have motivated much theoretical effort to analyze both the original Kitaev model as well as models with realistic extended interactions in magnetic fields.

On the theoretical side, it is known that without a magnetic field, the pure ferromagnetic (FM) and antiferromagnetic (AFM) versions of the Kitaev model are related by a unitary transformation and thus share the same topological properties. For both coupling signs, the Kitaev spin liquid (KSL) survives under a weak magnetic field, where it becomes gapped and hosts non-Abelian anyonic excitations [1]. The effects of a stronger field after suppressing the KSL state have however recently gained much theoretical interest due to the discovery of a field-induced *intermediate phase* (IP) in the AFM model [22,23]. This phase is separated from the low-field KSL and the high-field polarized state by phase transitions and could itself be a quantum spin liquid [24–28].

Motivated by these findings, (i) we perform a detailed analysis of the nature and dynamical response of the field-induced *intermediate phase* and neighboring phases in a family of Kitaev-based models related by hidden symmetries and duality transformations and (ii) we investigate the relevance of the IP for real materials, in particular for α-$RuCl_3$.

The paper is organized as follows. In Sec. II, we revise the properties of the Kitaev model and present numerical results for various dynamical response functions of the FM and AFM Kitaev model in uniform magnetic fields. This includes the dynamical spin-structure factor, which can be accessed by, e.g., inelastic neutron scattering (INS) or electron spin resonance (ESR) experiments, and dynamical bond correlations, that contribute to resonant inelastic x-ray scattering (RIXS) and Raman scattering. Furthermore, we probe directly static and dynamic flux-flux correlations that appear under field. In Sec. III A, we extend the parameter space to noncollinear magnetic fields, where we discuss hidden dual models. This allows us to effectively interpolate between the uniform-field behavior of the AFM and FM models with a continuous parameter. Numerically, we find that the field-induced IP of the AFM Kitaev model is highly unstable against certain nonuniform field rotations, and could manifest as a line of critical points in the parameter space of such generalized fields. In Sec. III B, we discuss the relevance of the field-induced IP of the AFM Kitaev model for real materials. By utilizing hidden symmetries in the parameter space of extended interactions, we show that the same IP can appear in realistic models for α-$RuCl_3$, that possess a *ferromagnetic* Kitaev coupling and additional interaction terms, for fields perpendicular to the honeycomb plane.

*kaib@itp.uni-frankfurt.de

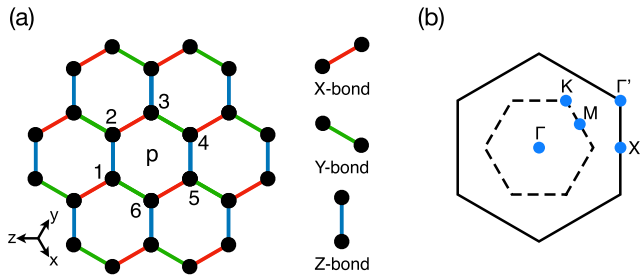

FIG. 1. (a) Honeycomb lattice with definitions of cubic axes x, y, z and bond types X, Y, Z. (b) High-symmetry k points in the first (dashed) and third Brillouin zone (solid border).

II. PURE KITAEV MODEL IN UNIFORM MAGNETIC FIELDS

A. Introduction and definitions

The Kitaev honeycomb model [1] is defined by a Hamiltonian consisting of bond-dependent Ising terms:

$$H_K = K \sum_{\langle ij \rangle_\gamma} S_i^\gamma S_j^\gamma, \tag{1}$$

where $\gamma \in \{x, y, z\}$ corresponds to the type of bond that connects i and j, according to Fig. 1(a). The classical version of the model exhibits an extensive degeneracy [29], that is lifted in the quantum model in favor of the KSL ground states. The exact solution of the quantum model can be achieved [1] by representing the spins via fermionic Majorana operators $\{b_j^x, b_j^y, b_j^z, c_j\}$ as $S_j^\gamma = \frac{i}{2} b_j^\gamma c_j$. This representation introduces a $\mathbb{Z}_2$ gauge redundancy; physical states are spanned by unique configurations of *matter* fermions, and $\mathbb{Z}_2$ *flux* degrees of freedom. The fluxes are associated with Wilson loop operators $\{W_L\}$, which commute with H_K and with each other. The shortest of such loops correspond to hexagonal plaquette operators $W_p = 2^6 S_1^x S_2^y S_3^z S_4^x S_5^y S_6^z$, where the site indices refer to those in Fig. 1(a). In the ground states, the flux density

$$\langle n_p \rangle \equiv \tfrac{1}{2}(1 - \langle W_p \rangle) \tag{2}$$

vanishes for every hexagonal plaquette p, and all excitations that modify the flux density are gapped. As a result, the ground state of the model can be written in terms of the solution of a free-fermion problem.

The exact solubility of the pure Kitaev model (1) has facilitated a deep understanding of its various response functions. For example, a single spin operator S_i^μ creates two fluxes on two neighboring plaquettes, in addition to excitations in the matter fermion sector. As a result, the dynamical spin-structure factor (DSSF)

$$\mathcal{S}(\mathbf{k}, \omega) = \sum_{\mu=x,y,z} \int dt\, e^{-i\omega t} \left\langle S_{-\mathbf{k}}^\mu(t)\, S_{\mathbf{k}}^\mu(0) \right\rangle \tag{3}$$

probes exclusively fluxful excitations. Given that W_p commutes with H_K, the fluxes are not dynamic, leading to a continuum that is both dispersionless [30] and gapped, with intensity only above the two-flux gap [31,32] of $\Delta_f \simeq 0.065|K|$.

In addition to the DSSF, the dynamics of the bond operators $B_{ij} := S_i^\gamma S_j^\gamma$ and of the flux operators W_p represent further interesting probes of the KSL. We consider for the bond operators the correlation function

$$\mathcal{I}_X(\mathbf{k}, \omega) := \int dt\, e^{-i\omega t} \langle B_{-\mathbf{k}}(t)\, B_{\mathbf{k}}(0) \rangle, \tag{4}$$

$$B_{\mathbf{k}} := \frac{1}{N} \sum_i e^{i\mathbf{k}\cdot\mathbf{r}_i} \sum_{\gamma=x,y,z} S_i^\gamma S_{\gamma(i)}^\gamma, \tag{5}$$

where $\gamma(i)$ is the nearest neighbor of i along a γ bond and N is the number of sites. Since $[B_{\mathbf{k}}, W_p] = 0$, for the pure Kitaev model, the correlation function $\mathcal{I}_X(\mathbf{k}, \omega)$ probes only dispersive fermionic matter excitations in the flux-free sector [33], revealing gapless modes (with vanishing intensity) at $\mathbf{k} = \Gamma$ and $\mathbf{k} = \mathrm{K}$ that reflect the Dirac spectrum of the underlying spinons [1]. Interestingly, $\mathcal{I}_X(\mathbf{k}, \omega)$ constitutes the main contribution to the spin-conserving channel of the resonant inelastic x-ray scattering (RIXS) intensity [33] and is therefore experimentally relevant. For $\mathbf{k} = \Gamma$, $\mathcal{I}_X(\Gamma, \omega)$ also contributes to Raman scattering [34]. Finally, we define the dynamical flux-structure factor

$$\mathcal{W}(\mathbf{k}, \omega) := \int dt\, e^{-i\omega t} \langle W_{-\mathbf{k}}(t)\, W_{\mathbf{k}}(0) \rangle, \tag{6}$$

$$W_{\mathbf{k}} := \frac{1}{N/2} \sum_p^{N/2} e^{i\mathbf{k}\cdot\mathbf{r}_p} W_p. \tag{7}$$

In the pure Kitaev model, $\mathcal{W}(\mathbf{k}, \omega)$ has no intensity at finite ω, reflecting that the ground state is an eigenstate of W_p. However, generic perturbations to H_K may lead to dynamics in W_p, as discussed below.

In this work, we focus on the effect of additional magnetic fields:

$$H = H_K - \sum_i \mathbf{h}_i \cdot \mathbf{S}_i \tag{8}$$

Previous works have focused primarily on uniform fields where $\mathbf{h}_i$ is equal at every site. For example, for weak uniform fields in the [111] direction, Kitaev employed perturbative arguments to show the appearance of a gap in the matter fermion spectrum, producing isolated bands that carry a nonzero Chern number [1]. It should be noted, since the magnetic fields lead to mixing of the zero-field flux and matter sectors and introduce a finite $\langle n_p \rangle$, that there are some ambiguities in the discussion of the excitations at finite field. Analogous to Kitaev's approach, one can consider perturbatively dressing the flux operators such that the ground state remains in the flux-free sector [35]. However, this approach remains valid only within the KSL phase. Instead, when considering general (nonuniform) fields, there is a conceptual advantage to studying the undressed operator B_{ij} and W_p. This is because models with different field configurations and/or signs of the Kitaev coupling K can be related by duality transformations that commute with these operators, leaving the dynamical response functions $\mathcal{I}_X(\mathbf{k}, \omega)$ and $\mathcal{W}(\mathbf{k}, \omega)$ invariant (Appendix A). Unless otherwise stated, we refer to undressed operators throughout this manuscript.

The fate of the Kitaev model in uniform fields beyond the perturbative regime has been the subject of much recent interest. Various numerical studies [22,23,27,36] have showed that the FM ($K < 0$) and AFM ($K > 0$) versions of the Kitaev

model display rather different behavior under a uniform field. The FM model exhibits a single phase transition as a function of field strength at $h_c^{FM} \approx 0.03|K|$, qualitatively independent of field direction [27]. The transition occurs directly to a *quantum paramagnet* (QPM) phase, that is smoothly connected to the *fully polarized state* of the $h \to \infty$ limit. In contrast, recent studies of the AFM model have found an additional *intermediate phase* [22–27] (IP) for fields along the cubic [111] direction, in the range $h_{c1}^{AFM} < h < h_{c2}^{AFM}$, with $h_{c1}^{AFM} \approx 0.4K$ and $h_{c2}^{AFM} \approx 0.6K$. The IP is thought to be gapless in the thermodynamic limit [22–27]. Consequently, descriptions of the IP in terms of various types of spin liquids have been proposed [24–28]. Interestingly, the stability of the IP also appears to depend on the orientation of the field [27]; for fields along [001] in the AFM Kitaev model, Majorana mean-field studies [37,38] found a possibly different field-induced phase.

We argue that the contrast between the FM and AFM models under uniform fields can be anticipated by considering the classical limit; in the case of FM coupling, a finite field instantly selects the polarized state out of the classically degenerate spin configurations [39], suggesting a critical field of $h_{c,class}^{FM} = 0$. For AFM coupling, the classical degeneracy is retained [39] up to a field of $h_{c,class}^{AFM} = K$, as the polarized state does not fulfill the AFM spin-spin correlations preferred by the coupling. In the *quantum* Kitaev models (both FM and AFM), the stability of the KSL is determined instead by the relative strength of the field compared to the magnitude of the zero-field flux gap Δ_f, which represents an additional emergent low-energy scale. Independent of the sign of K, excitations carrying finite flux acquire a dispersion on the order of h. Intuitively, suppression of the zero-field spin liquid likely occurs when this dispersion exceeds the zero-field flux gap, leading to a proliferation of fluxes at a critical field strength of $h_c \sim \Delta_f$, implying a finite stability of the KSL. For the AFM model, the fact that the classical degeneracy is retained up to larger fields $h_{c,class}^{AFM} \gg \Delta_f$ suggests the possibility of an additional intermediate field regime in the quantum model where neither the KSL nor the polarized phase are the ground state, in line with the appearance of the IP. The extension of these ideas to nonuniform fields is discussed in Sec. III A.

B. Ferromagnetic Kitaev model

In order to study the phenomenology of a direct transition between the KSL and the field-polarized phase, we first consider the FM Kitaev model ($K < 0$) in a uniform magnetic field $\mathbf{h} \parallel [111]$, described by Eq. (8). All shown results were obtained on the 24-site periodic cluster shown in Fig. 1(a) via exact diagonalization (ED), with a broadening in frequency of $0.025|K|$ applied to the dynamical response functions. Other studied field directions (not shown) including $[1\bar{1}0]$, $[11\bar{2}]$, and [001] yield qualitatively similar response.

The evolution of the dynamical spin-structure factor $\mathcal{S}(\mathbf{k}, \omega)$ is shown in Figs. 2(a) and 2(b) for $\mathbf{k} = \Gamma$ and K, respectively. Starting from the KSL at $h = 0$, the applied field leads to broadening of the intense band of spin excitations that appear just above the (zero-field) two-flux gap in the range $\omega \sim 0.1$–$0.3\ |K|$. This broadening can be attributed to the field-induced dispersion for the fluxful excitations, which is expected to occur through both the mixing of flux and matter

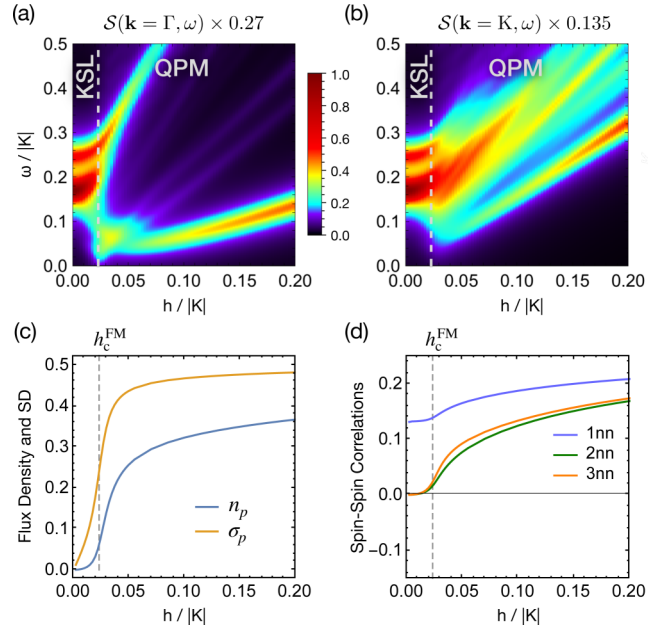

FIG. 2. FM Kitaev model under [111] field. (a), (b) Low-frequency dynamical spin-structure factor at selected k points. Poles at $\omega = 0$ are not shown. (c) Flux density $\langle n_p \rangle$ and standard deviation (SD) of the local flux density $\sigma_p = \sqrt{\langle {n_p}^2 \rangle - \langle n_p \rangle^2}$. (d) Static spin-spin correlations in real space. 1nn, 2nn, 3nn denote $\langle \mathbf{S}_i \cdot \mathbf{S}_j \rangle$ on first-, second-, and third-nearest neighbors, respectively.

sectors, as well as the hopping of the dressed fluxes. The broadening ultimately leads to the closure of the spin gap at $h_c^{FM} \sim 0.02|K| \sim \Delta_f$. Coming from high-field, semiclassical spin-wave approaches would suggest a softening of magnons at all wave vectors on approaching the spin liquid [40]. As a result, the spin excitation gap may close everywhere in $\mathbf{k}$-space simultaneously. For $h > h_c^{FM}$, the slope of the magnon energies with respect to field is smallest at $\mathbf{k} = \Gamma$ [compare Figs. 2(a) and 2(b)], as the minimal energy magnons exist at the zone center in the limit of large field.

The emergence of a large flux density under field can be seen in the evolution of $\langle n_p \rangle$ shown in Fig. 2(c). While fluxes remain to be nearly absent in the KSL until the critical field h_c^{FM}, the average flux density and local flux density fluctuations measured by $\sigma_p = \sqrt{\langle {n_p}^2 \rangle - \langle n_p \rangle^2}$ rapidly increase at the transition into the QPM. Remarkably, $\langle n_p \rangle$ stays significantly below the limit [41] for the classical polarized state, $\lim_{h\to\infty} \langle n_p \rangle = \frac{13}{27} \simeq 0.48$, for a wide range of field strengths, implying significant quantum fluctuations in the QPM. The latter are also evident from long-range spin-spin correlations developing only gradually above h_c^{FM}, cf. Fig. 2(d).

Since W_p commutes with H_K, the dynamics of the fluxes are mostly controlled by the field strength. In the asymptotically polarized region at high field, the dynamical flux-structure factor $\mathcal{W}(\mathbf{k}, \omega)$ [see Figs. 3(a) and 3(b) for $\mathbf{k} = \Gamma$, K respectively] features a series of excitation bands corresponding to n-spin flips that do no alter $\langle S_i^\gamma S_j^\gamma \rangle$. On approaching h_c^{FM} from above, these excitations collapse into a narrow frequency range on the scale of the zero-field flux gap Δ_f. Importantly, since h_c^{FM}, $\Delta_f \ll |K|$, the flux dynamics near the

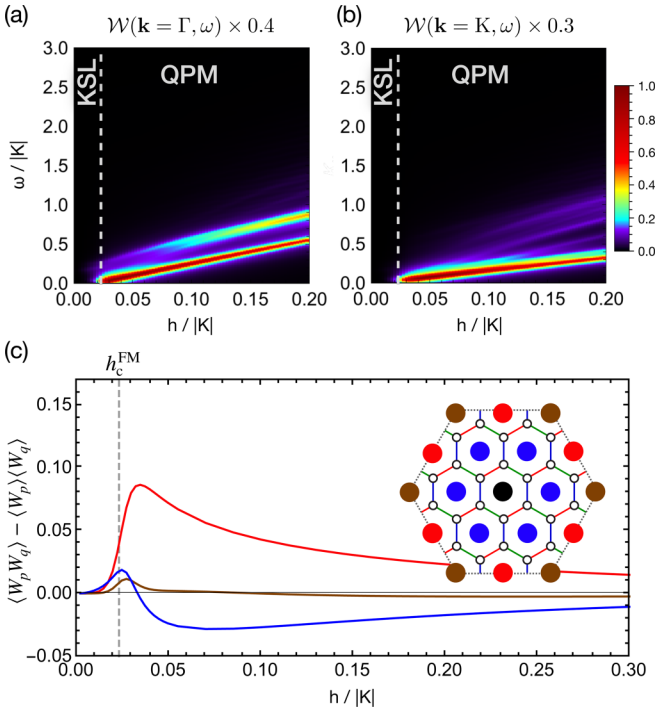

FIG. 3. Flux correlations in the FM Kitaev model under [111] field. (a), (b) Dynamical flux-structure factor $\mathcal{W}(\mathbf{k},\omega)$. (c) $\langle W_pW_q\rangle - \langle W_p\rangle\langle W_q\rangle$, where each line color refers to the relative position of the respective plaquette p to the black plaquette q shown in the inset.

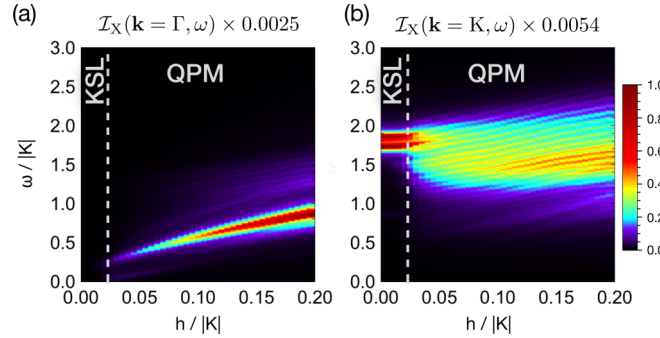

FIG. 4. Spin-conserving RIXS intensity $\mathcal{I}_{\mathrm{X}}(\mathbf{k},\omega)$ in the FM Kitaev model under [111]-field.

critical field are exceedingly slow compared to the timescales for other excitations. As a result, the finite flux-density state just above the critical field may be discussed in terms of nearly static fluxes, making it useful to consider the real-space static flux-flux correlations.

The static flux-flux correlations $\langle W_pW_q\rangle - \langle W_p\rangle\langle W_q\rangle$ are shown in Fig. 3(c). Deep in the KSL, the magnetic field creates virtual pairs of fluxes on neighboring plaquettes, which then may hop to adjacent plaquettes. However, flux pairs remain bound to each other due to the finite flux gap. As a result, fluctuations around the flux-free ground state lead to positive real-space correlations that decay with increasing plaquette separation. In contrast, for $h > h_c^{\mathrm{FM}}$, the correlations are markedly different, likely reflecting effective interactions between fluxes that exist in finite density. The energetics of different flux configurations was studied first by Kitaev [1], and later by Lahtinen *et al.* [42–44]. In analogy with vortices in $p+ip$ superconductors, each flux binds a Majorana c-fermion [1,45] under applied field. Minimizing the energy of the Majorana bound states for pairs of fluxes leads to effective flux-flux interactions, which prefer that two fluxes are located on second-neighbor plaquettes parallel to a bond, for example. The correlations observed near the critical field are consistent with flux patterns that minimize these interactions. Indeed, provided that the dynamics of the fluxes remain slow compared to the c-fermions, the essential effects of such bound states are likely to be preserved. While the spatial range of flux-flux correlations is difficult to diagnose from finite-size calculations, we note that a state with true long-range staggered flux order [46] would necessarily break additional lattice symmetries, and would therefore be distinct from the fully polarized state. Since no signatures of an additional phase transition have been detected numerically [22,23], it is likely that the flux-flux correlations retain a finite range in the thermodynamic limit. Therefore the large flux-flux correlations observed in these calculations do not appear to reflect the formation of a long-range ordered flux (vison) crystal of the type studied in Ref. [46].

The fate of the matter fermions can be diagnosed from dynamical bond correlations. We therefore discuss the spin-conserving channel of the resonant inelastic x-ray scattering (RIXS) intensity $\mathcal{I}_{\mathrm{X}}(\mathbf{k},\omega)$, as defined in Eq. (4). For completeness, we note that the form of the operator in Eq. (5) neglects additional contributions to the response that can appear at finite field related to differences in g tensors between core and valence shell states. For a direct RIXS process in the first-order fast-collision approximation (employed in Ref. [33]), the RIXS operator gains an additional single-spin term under field, with relative magnitude $\sim|(\mathbf{g}_{\mathrm{c}}-\mathbf{g}_{\mathrm{v}})\cdot\mathbf{h}|/|K|$, where $\mathbf{g}_{\mathrm{c}}$ and $\mathbf{g}_{\mathrm{v}}$ are the g tensors of the core and valence shells that are involved in the RIXS process. Under the assumption that these g tensors are similar, and for fields h smaller than $|K|$, the main contribution to the spin-conserving RIXS intensity should therefore still be described by $\mathcal{I}_{\mathrm{X}}(\mathbf{k},\omega)$ under finite fields.

Exact diagonalization results for $\mathcal{I}_{\mathrm{X}}(\mathbf{k},\omega)$ are shown in Figs. 4(a) and 4(b) for $\mathbf{k}=\Gamma$ and K respectively. In the zero-field KSL, the majority of the spectral weight is represented by two-fermion excitations at energies $\omega \gtrsim 0.8|K|$ at all wave vectors, as in Fig. 4(b). The $\mathbf{k}$ points Γ, and Γ' are an exception, as the intensity vanishes at zero field due to $[B_{\mathbf{k}=\Gamma,\Gamma'}, H_K]=0$ [Fig. 4(a)]. The discreteness of these features in our calculations can be attributed to finite size effects, but their energy range agrees with exact calculations at zero field [33]. Above h_c^{FM}, the former sharp excitations of the KSL significantly broaden, consistent with strong scattering from the finite density of fluxes introduced by h. As a result, the matter fermions cease to be well-defined excitations almost immediately upon entering the QPM phase above h_c^{FM}. In contrast to the AFM Kitaev model discussed below, the broad excitation bands, that emerge above h_c^{FM}, begin at frequencies similar to their corresponding zero-field two-fermion excitations. At high fields strengths $h \gg h_c^{\mathrm{FM}}$, the QPM can eventually be described as asymptotically polarized. Since

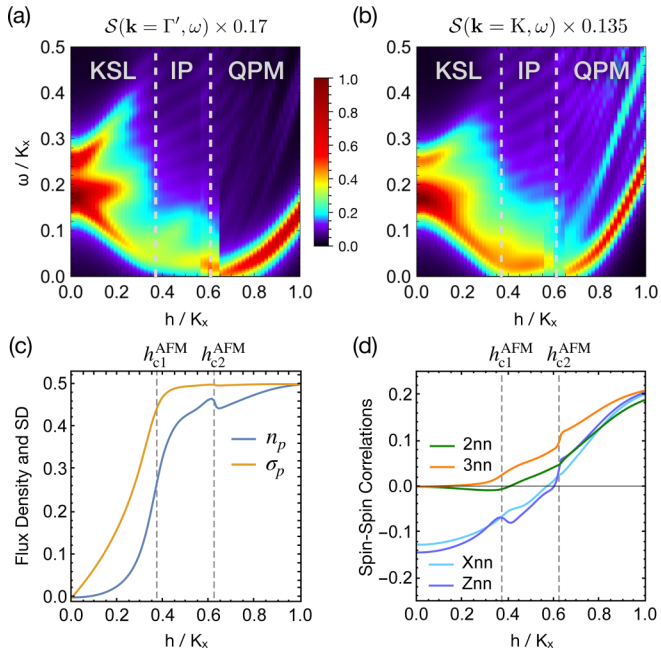

FIG. 5. AFM Kitaev model with $K_x = K_y, K_z = 1.05K_x$ under [111] field. (a), (b) Low-frequency dynamical spin-structure factor. (c) Flux density $\langle n_p \rangle$ and standard deviation (SD) of the local flux density $\sigma_p = \sqrt{\langle {n_p}^2 \rangle - \langle n_p \rangle^2}$. (d) Static spin-spin correlations in real space. Xnn and Znn denote $\langle \mathbf{S}_i \cdot \mathbf{S}_j \rangle$ on X and Z bonds, respectively.

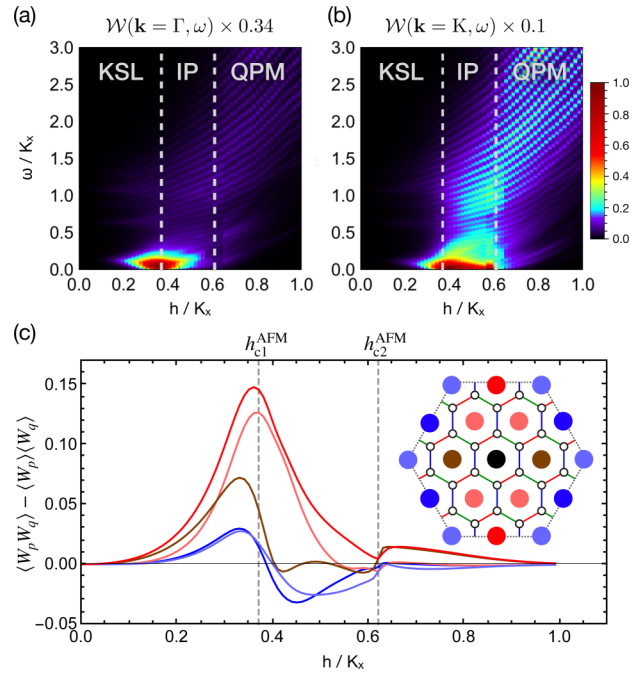

FIG. 6. Flux correlations in the AFM Kitaev model with $K_x = K_y, K_z = 1.05K_x$ under [111] field.

the bond-bond correlations probe multispin-flip excitations, they become increasingly expensive under applied field and, accordingly, the broad bands of excitations shift to higher energies with increasing h.

C. Antiferromagnetic Kitaev model

We now consider the AFM Kitaev model in uniform [111] field. To mitigate some finite-size effects in the *intermediate phase* [47], we slightly break C_3 symmetry by choosing the coupling strength on Z bonds (K_z) stronger than that on X and Y bonds: $K = K_x = K_y, K_z = 1.05K_x$. Dynamic and static response functions computed via ED are shown in Figs. 5 to 7.

For the dynamical spin-structure factor shown in Figs. 5(a) and 5(b) at $\mathbf{k} = \Gamma', \mathrm{K}$, we reproduce the results of Ref. [27]. At small h, the intense excitations at the flux gap broaden significantly, with the lower bound reaching nearly zero frequency at $h_{c1}^{AFM} \approx 0.4K$. Unlike a continuous transition to a spin-ordered phase [48], the spin gap appears to close everywhere in k space simultaneously at h_{c1}^{AFM}. The spin gap remains small within ED resolution up to the second critical field $h_{c2}^{AFM} \approx 0.6K$. This observation has previously been interpreted as the presence of gapless spin excitations in the IP in the thermodynamic limit [23,27].

Similar to the FM model, the vanishing energy difference between different flux sectors at h_{c1}^{AFM} allows fluxes to proliferate. As a result, the first critical field marks a rapid increase in the average flux density n_p, as well as in local flux-density fluctuations σ_p, see Fig. 5(c). In contrast, both quantities change very little at the second critical field h_{c2}^{AFM}.

In the IP, the dynamical flux-structure factor $\mathcal{W}(\mathbf{k}, \omega)$, shown in Figs. 6(a) and 6(b), displays a broad continuum in the energy range $\omega \sim 0$ to $3K$. However, much of the spectral weight is concentrated at small frequencies $0 \lesssim \omega \lesssim 0.1K$, on the same scale as the zero-field flux gap. This indicates that the flux fluctuations—while large in amplitude σ_p—occur primarily on relatively *slow* timescales throughout the IP. This is in contrast to neighboring ordered phases of the KSL, which can be induced by, e.g., an additional Heisenberg term, where we find the spectral weight of $\mathcal{W}(\mathbf{k}, \omega)$ to be concentrated at higher frequencies, with negligible weight near $\omega \approx 0$. Likewise, in the QPM phase in Figs. 6(a) and 6(b) for $h > h_{c2}^{AFM}$, the low-frequency intensity in $\mathcal{W}(\mathbf{k}, \omega)$ is rapidly suppressed. Here, the opening of a gap at h_{c2}^{AFM} shifts all excitations to higher energies with increasing field. Similar to the FM model near h_c^{FM}, the IP features pronounced modulation of the static flux-flux correlations $\langle W_p W_q \rangle - \langle W_p \rangle \langle W_q \rangle$ in real space, shown in Fig. 6(c). In this case, the correlations show a stripy

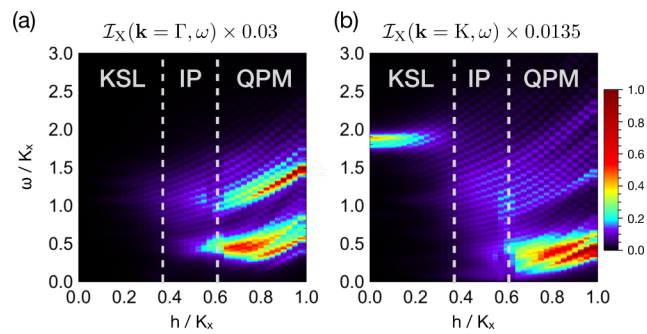

FIG. 7. Spin-conserving RIXS intensity $\mathcal{I}_X(\mathbf{k}, \omega)$ in the AFM Kitaev model with $K_x = K_y$, $K_z = 1.05K_x$ under [111] field.

pattern, the orientation of which is selected by the choice of $K_z > K_x, K_y$. These correlations are a property of the IP, and are largely suppressed upon approaching h_{c2}^{AFM}.

The spin-conserving RIXS intensity $\mathcal{I}_X(\mathbf{k}, \omega)$ of the AFM Kitaev model under field is shown in Fig. 7. Here, the response under field differs significantly from the FM Kitaev model due to the negative sign of static bond correlations $\langle S_i^\gamma S_j^\gamma \rangle$ in the low-field KSL, cf. Figs. 2(d) and 5(d). Upon entering the IP at h_{c1}^{AFM}, the discrete two-fermion excitations of the KSL observed in ED dissolve into a broad band with no distinct frequency or momentum dependence [compare Figs. 7(a) and 7(b)], confirming that the c-fermions are strongly perturbed by the presence of the fluxes. At $h \sim h_{c1}^{\mathrm{AFM}}$, a significant portion of spectral weight in $\mathcal{I}_X(\mathbf{k}, \omega)$ remains at high frequencies. However, in contrast to the FM model, part of the broad band shifts downward with increasing h, as the magnetic field reduces the energy cost for flipping the signs of $\langle S_i^\gamma S_j^\gamma \rangle$. Finally, at $h = h_{c2}^{\mathrm{AFM}}$, the band is driven to $\omega \approx 0$ at all wave vectors. Consistently, the static nearest-neighbor spin-spin correlations rapidly reverse sign upon leaving the IP, as shown in Fig. 5(d).

III. STABILITY OF THE INTERMEDIATE PHASE IN EXTENDED MODELS

A. Noncollinear fields

As discussed in Sec. II, the presence of the IP in the AFM Kitaev model under a uniform field can be anticipated from two observations: (i) a finite field rapidly induces flux density fluctuations (suppressing the KSL) at $h \sim \Delta_f$, but (ii) does not immediately lift the extensive classical degeneracy. For this reason, a quantum spin liquid phase at intermediate fields can be anticipated. This argument can be extended to include general site-dependent fields defined by

$$H_f = -\sum_i h_i^x S_i^x + h_i^y S_i^y + h_i^z S_i^z. \tag{9}$$

For field configurations that do not couple to any classically degenerate state [29], the product of the γ component of the local fields on all γ bonds must satisfy

$$h_i^\gamma = \mathrm{sgn}(K)\, h_j^\gamma, \tag{10}$$

which serves as a *necessary* condition for maintaining the classical degeneracy at finite field. While a uniform field fulfills this only in the AFM model ($K > 0$), certain noncollinear field configurations satisfy it in the FM model, suggesting that the IP may be also induced by such fields in the FM model. In fact, as discussed in Appendix A, the AFM Kitaev model under uniform [111] field is exactly dual to the FM model under the four-sublattice "tetrahedral" field pictured in Fig. 8. Similarly, the AFM model under the four-sublattice field is dual to the FM model under uniform [111] field.

These dualities allow us to consider a series of models that interpolate between those possessing the IP, and those where a direct transition occurs between the KSL and the QPM. To this end, we consider the phase diagram of the AFM Kitaev

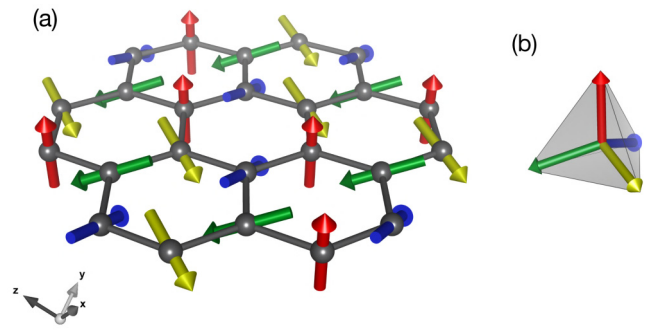

FIG. 8. (a) Site-dependent directions of the four-sublattice tetrahedral field that acts on H_K in the same way as a uniform field does on $-H_K$. The relative orientations of the local fields match those of the vertex corners of a tetrahedron, as shown in (b).

model with site-dependent fields:

$$H(h, \phi) = H_{K,\mathrm{AFM}} - h \sum_i \mathbf{h}_i(\phi) \cdot \mathbf{S}_i, \tag{11}$$

with local field directions $\mathbf{h}_i(\phi)$ defined by the sublattice pattern in Fig. 12(d), with

$$\mathbf{h}_i(\phi) = \frac{1}{\sqrt{3}} \begin{cases} (1,1,1), & \text{if } i \in \text{sublattice A} \\ (v,u,v), & \text{if } i \in \text{sublattice B} \\ (v,v,u), & \text{if } i \in \text{sublattice C} \\ (u,v,v), & \text{if } i \in \text{sublattice D} \end{cases}, \tag{12}$$

$$u(\phi) = \cos(\phi) + \sqrt{2}\sin(\phi), \tag{13}$$

$$v(\phi) = \cos(\phi) - \sin(\phi)/\sqrt{2}. \tag{14}$$

For this choice, $\mathbf{h}_i(\phi)$ rotates directly between a uniform [111] field (for $\phi = 0$), and the tetrahedral field shown in Fig. 8 (for $\phi = \arccos(-\frac{1}{3}) \equiv \phi_{\mathrm{tet}} \simeq 0.61\pi$). As introduced above, the model is dual to the FM Kitaev model in uniform [111] field for $\phi = \phi_{\mathrm{tet}}$. Eq. (10) becomes violated as soon as $\phi \neq 0$.

The phase diagram as a function of ϕ and h obtained via ED is shown in Fig. 9(a). Phase boundaries were identified from maxima in the second derivative of the ground state energy $-\partial_g^2 E_0$ and in the fidelity susceptibility

$$\chi_g = \frac{-2\log(|\langle\psi(g)|\psi(g+\delta g)\rangle|)}{(\delta g)^2}, \tag{15}$$

where we have varied both $g = h$ or $g = \phi$. The locations of these maxima are shown as black points in Fig. 9(a).

We first focus on the region for $\phi \geqslant 0$. As shown in the phase diagram, we find that the IP is very unstable against tetrahedral rotations, surviving only for the narrow range $\phi \lesssim 0.005\pi = 0.9^\circ$ in our $N = 24$ calculations. For all angles $\phi > 0.9^\circ$, a direct transition between the KSL and QPM is observed, with critical field h_c decreasing monotonically with rotation angle. The extent of the KSL and IP can be deduced from the behavior of the flux density, plotted in Fig. 9(b). In the KSL, n_p is suppressed, while in the IP this quantity is enhanced compared to adjacent phases. In Fig. 9(c), we show the behavior of the fidelity susceptibility χ_ϕ in the narrow region around $\phi \sim 0$. For $0.4 \lesssim \frac{h}{K} \lesssim 0.6$, the transition between the IP and the polarized phase occurs via level crossings on sweeping ϕ, signified by two divergencies in χ_ϕ at very small

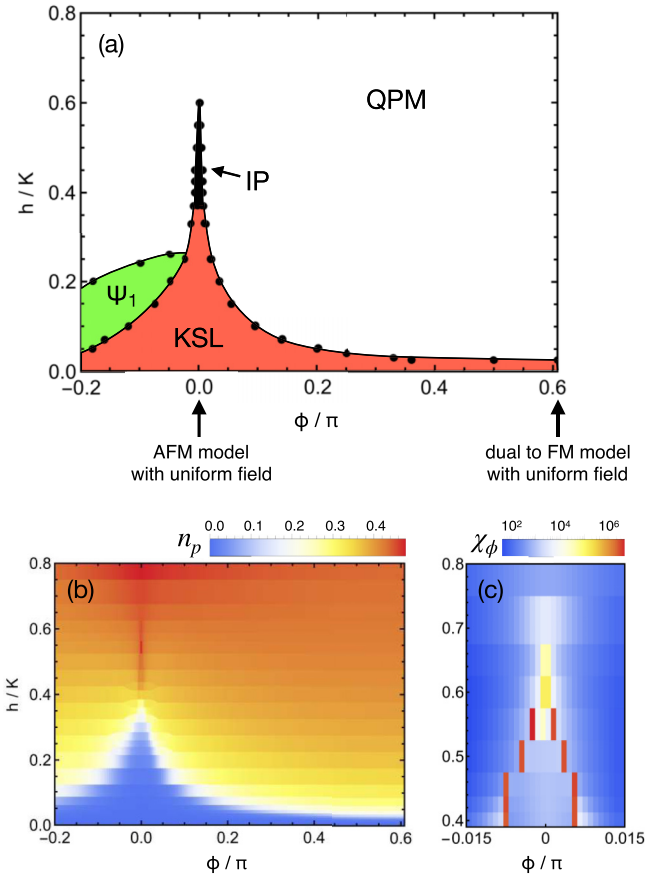

FIG. 9. (a) Phase diagram interpolating between the AFM Kitaev model under a uniform [111]-field ($\phi = 0$) and a model dual to the FM model under a uniform [111] field ($\phi = \phi_{\text{tet}} \simeq 0.61\pi$) via Eqs. (11) to (14). Black points depict maxima in the fidelity susceptibility. (b) $\langle n_p \rangle$ [Eq. (2)]. (c) Fidelity susceptibility [Eq. (15)] with respect to ϕ, close to the limit of uniform fields $\phi = 0$. Calculated with $\delta\phi = 0.005\pi$. Note that the color scale is logarithmic.

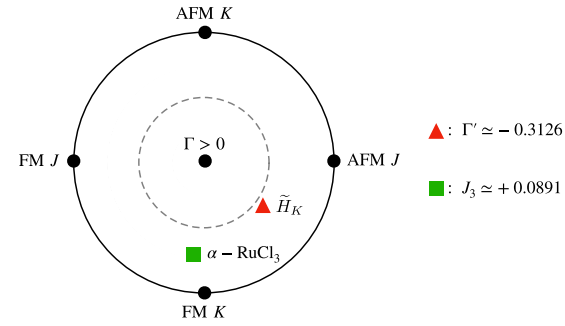

FIG. 10. (J, K, Γ)-parameter space for $\Gamma > 0$. We adopt the parametrization of Refs. [49,57], such that $J = \sin\vartheta\cos\varphi$, $K = \sin\vartheta\sin\varphi$, $\Gamma = \cos\vartheta$, where φ is the polar angle and ϑ is proportional to the distance from the center, reaching $\vartheta = \pi/4$ at the dashed circle and $\vartheta = \pi/2$ at the outer circle. The black dots show models where only one type of coupling is present. The triangle and the square show the projected positions of the hidden AFM Kitaev model [Eq. (18)] and of the α-RuCl_3 model [Eq. (19)], respectively. Additional couplings that are not encoded in (φ, ϑ) are given on the right side in units of $\sqrt{J^2 + K^2 + \Gamma^2}$.

negative and positive ϕ. For $h \gtrsim 0.6K$, the divergences meet and are rapidly suppressed.

While the above results suggest the IP has a very small—but finite—extent with respect to ϕ, we note that the energy spectra in finite-size calculations are necessarily discrete. The level crossings shown in Fig. 9(c) can therefore not happen instantly at $\phi = 0$ in our calculations, but must appear after a finitely large perturbation to the Hamiltonian. Provided that the IP is gapless in the thermodynamic limit, as concluded in Refs. [22–27], the critical ϕ values may scale to zero as the finite-size gap closes. In our calculations on 24 sites, the narrow width of the IP is controlled by the relative scale of the energy gaps $\sim 0.01K$ between the ground state and lowest excited states at $\phi = 0$. For this reason, we cannot rule out a scenario in which the IP is reduced to a line of critical points in the (h, ϕ) plane of Fig. 9(a) in the thermodynamic limit, with no finite extent in the ϕ-direction. This suggests an intriguing instability of the IP with respect to nonuniform field rotations, which coincides with the instability of the classical degeneracy in the model formulated by Eq. (10).

Finally, we comment briefly on a phase detected for negative ϕ. The region of this additional phase [named Ψ_1 in Fig. 9(a)] can be outlined clearly by maxima in χ_g and $-\partial_g^2 E_0$. From the static spin-structure factor, we can not identify a dominant ordering wave vector. Within the discrete spectra of the ED calculation, the gap throughout the region of Ψ_1 is on the order of $0.02K$, so that one could speculate about a potential gaplessness in the thermodynamic limit. In this respect, it has similarities to the IP, however we do not find Ψ_1 to be smoothly connected to the IP in the considered parameter space on the basis of χ_g and $-\partial_g^2 E_0$. Furthermore $\langle n_p \rangle$ in the Ψ_1 phase is significantly lower than in the IP, yet still distinctly above that of the KSL, see Fig. 9(b).

B. Extended interactions

To date, material realizations of Kitaev-like Hamiltonians have been sought in a number of spin-orbital coupled transition metal compounds including α-RuCl_3, $\mathrm{Na_2IrO_3}$, and various polymorphs of $\mathrm{Li_2IrO_3}$. In such materials, the minimal nearest-neighbor couplings can be parameterized [49,50]:

$$H_{JK\Gamma\Gamma'} = \sum_{\langle ij\rangle_\gamma} J\,\mathbf{S}_i\cdot\mathbf{S}_j + K\,S_i^\gamma S_j^\gamma + \Gamma\left(S_i^\alpha S_j^\beta + S_i^\beta S_j^\alpha\right) + \Gamma'\left(S_i^\alpha S_j^\gamma + S_i^\gamma S_j^\alpha + S_i^\beta S_j^\gamma + S_i^\gamma S_j^\beta\right), \qquad (16)$$

where $\gamma \in \{x, y, z\}$ corresponds to the type of bond connecting sites i and j, and (α, β, γ) is always a permutation of (x, y, z). While the precise determination of magnetic Hamiltonians for the candidate materials poses an ongoing challenge, the Kitaev exchange has been shown to be of ferromagnetic type (FM, $K < 0$), on grounds of the idealized microscopic mechanism [2], *ab initio* studies [11,50–56] and experimental analyses [9,57–62]. While we have discussed in Sec. III A and Appendix A that the field-induced IP can be realized in the FM Kitaev model, this requires noncollinear and staggered fields that are unlikely to be available in experiments on real materials. At first glance, this puts into

question the relevance of the physics of the IP to real materials.

From this viewpoint, it is useful to note the presence of *hidden* Kitaev points in the extended (J, K, Γ, Γ')-parameter space [cf. Eq. (16)], which are implied by transformations discussed in Ref. [57]. In particular, a π rotation of all spin-operators around the [111] axis is defined by

$$\mathcal{R} : (\tilde{x}, \tilde{y}, \tilde{z})^{\intercal} = \frac{1}{3}\begin{pmatrix} -1x + 2y + 2z \\ +2x - 1y + 2z \\ +2x + 2y - 1z \end{pmatrix}. \tag{17}$$

Applying this transformation to the pure AFM Kitaev model H_K $(K = +1)$ leads to a Hamiltonian $\widetilde{H}_K = \mathcal{R} H_K \mathcal{R}^{-1}$, that is of the (J, K, Γ, Γ') form with parameters

$$\widetilde{H}_K : \quad (\tilde{J}, \tilde{K}, \tilde{\Gamma}, \tilde{\Gamma}') = \left(+\frac{4}{9}, -\frac{1}{3}, +\frac{4}{9}, -\frac{2}{9}\right). \tag{18}$$

Importantly, the signs of all anisotropic couplings (i.e., $K < 0$, $\Gamma > 0$ and $\Gamma' < 0$) at this hidden AFM Kitaev point are compatible with microscopic mechanisms relevant to known Kitaev materials [49,55]. Such couplings are, in principle, realizable in real materials. The static $\mathbb{Z}_2$ gauge field for the KSL ground state of $\widetilde{H}_K$ is related to new flux operators $\widetilde{W}_p = \mathcal{R} W_p \mathcal{R}^{-1}$. Since $\mathcal{R}$ commutes with the Zeeman term of a [111] field, $\widetilde{H}_K$ hosts the IP under *uniform* fields. In Fig. 10, we show the position of the hidden AFM Kitaev point $\widetilde{H}_K$ projected into the (J, K, Γ)-parameter space.

Since both the KSL and the IP at the original AFM Kitaev point have finite extents when adding additional interactions to H_K [27,49,63] these phases must also have finite extent around the *hidden* Kitaev model $\widetilde{H}_K$. It is therefore interesting to explore as to what extent these phases might be proximate to the phases of real materials. To that end, we take as a representative for real materials the *ab initio*-guided minimal model of Ref. [65] for α-$RuCl_3$:

$$H_{\mathrm{RuCl}} : \ (J, K, \Gamma, J_3) = (-0.5, -5, +2.5, +0.5)\ \mathrm{meV}, \tag{19}$$

where J_3 stands for third-nearest-neighbor Heisenberg coupling. We then consider models:

$$H(\xi, \mathbf{h}) = (1 - \xi)\, \widetilde{H}_K + \xi \frac{1}{C} H_{\mathrm{RuCl}} - \sum_i \mathbf{h} \cdot \mathbf{S}_i, \tag{20}$$

which interpolate between the hidden AFM Kitaev point ($\xi = 0$) and the α-$RuCl_3$ model ($\xi = 1$) under uniform fields $\mathbf{h}$. We set $C = 8.5$ meV for comparable energy scales. H_{RuCl} has been shown to be consistent with many experimental aspects of α-$RuCl_3$ [13,17,64–67]. While the model can certainly still be further fine-tuned [67], we assert that the relative direction in parameter space between $\widetilde{H}_K$ and α-$RuCl_3$ can be described reasonably well with H_{RuCl}.

In Figs. 11(a)–11(f), we show the ground state phase diagrams of $H(\xi, \mathbf{h})$ for three different directions of $\mathbf{h}$, going from in-plane ($\mathbf{h} \parallel b = [1\bar{1}0]$) to out-of-plane ($\mathbf{h} \parallel c^* = [111]$) fields. Phase boundaries were determined from ED on the high-symmetry 24-site cluster, by tracking maxima in χ_g [Eq. (15)] and in $-\partial_g^2 E_0$ with $g = h$ or $g = \xi$. The physical B-field in tesla is related to our natural units as $\mathbf{B} = C\mu_{\mathrm{B}}^{-1}\mathbf{g}^{-1}\mathbf{h}$, shown on the right-hand axes in Fig. 11 for the g-tensor estimate of Ref. [64].

On the described path through parameter space, the zigzag phase of H_{RuCl} is found to be a (direct) neighbor of the hidden KSL phase, meeting it at $\xi \simeq 0.04$ for $h = 0$. With increasing field strength, this phase boundary bends towards smaller ξ, see Figs. 11(b), 11(d) and 11(f). Hence, no model exists on the path where an external field can suppress zigzag order in favor of a field-induced KSL state, unlike the path considered in Ref. [70], where the KSL can be field-induced for field directions close to [111]. For the models considered here, the stability of the KSL region is found to be qualitatively independent of field direction.

In contrast, the stability of the field-induced IP depends crucially on the field direction. Even for $\xi = 0$ at the pure (hidden) Kitaev model, the IP is not induced for all uniform field directions, as is the case for the direction shown in Figs. 11(c) and 11(d). For most field directions where the IP is observed, it is found to be less stable than the KSL against additional interactions introduced by a finite ξ, as in Figs. 11(a) and 11(b), so that it cannot generally be field-induced from a zigzag ground state either. Remarkably, however, we find exclusively for the out-of-plane field direction $[111] = c^*$, that the IP extends far through parameter space, reaching even the H_{RuCl} model at $\xi = 1$ at high fields, see Figs. 11(e) and 11(f). This result applies only for fields very near to the [111] direction [71]. Upon rotating $\mathbf{h}$ by small angles of $\lesssim 10^\circ$ away from [111], the extended region shrinks quickly, such that the extent of the IP with respect to ξ becomes qualitatively similar to that in Fig. 11(b). We remark the presence of level crossings between quasidegenerate states within the IP region on the high-symmetry cluster for [111] fields [47]. These are expected to be inconsequential finite-size artifacts, since similar features in the nearest-neighbor Kitaev-Heisenberg vanish on larger clusters accessible by density-matrix renormalization group (DMRG) methods [72].

While the particular model H_{RuCl} does not host any field-induced phase between the zigzag and polarized phases on the classical level [73], a candidate field-induced classical phase that is nearby in parameter space would be the "AF vortex" phase of Ref. [39]. Then, linear spin-wave theory within the QPM would however predict a gap closing at $\mathbf{q} = \mathrm{K}$ upon reaching the AF vortex phase coming from high fields, which is inconsistent with the dynamical response we observe within ED for H_{RuCl} upon reaching the IP (Appendix B). We therefore find that the behavior of H_{RuCl} under a [111] field in ED is inconsistent with either classical scenarios; an intermediate ordered phase or a direct transition between zigzag and polarized [73].

Our results indicate that the IP is present in α-$RuCl_3$ for strictly *out-of-plane* [111] fields. The IP is therefore unlikely to be linked to various experimental observations in α-$RuCl_3$ for fields tilted significantly *away* from [111] and *in-plane* fields that have been interpreted in terms of a field-induced quantum spin liquid independently [14–16,18,20].

IV. SUMMARY AND OUTLOOK

We have presented a detailed numerical study of Kitaev-based models in both uniform and general noncollinear fields, which provide a broad new theoretical realm to probe the phenomenology of this model. By exploiting the large number

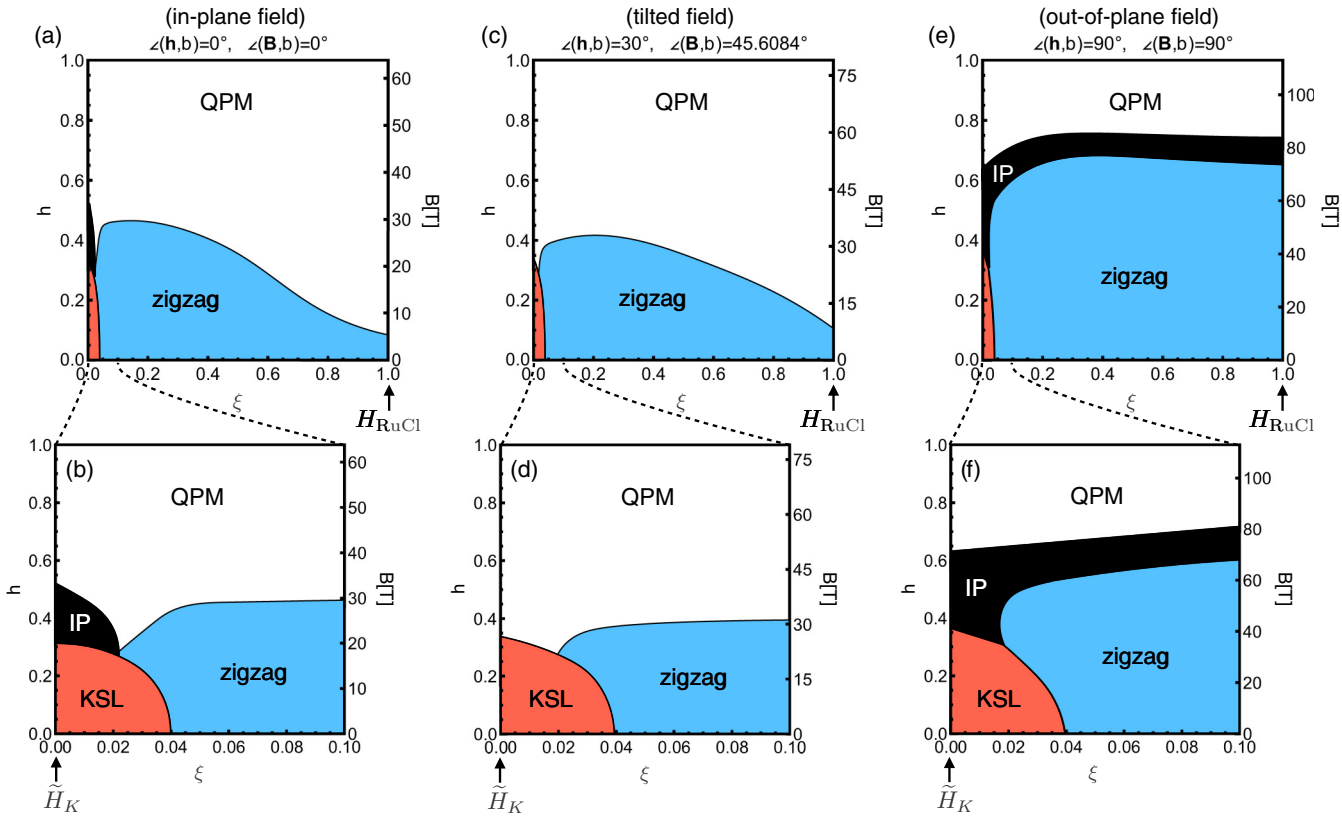

FIG. 11. Phase diagrams of $H(\xi, \mathbf{h})$ from Eq. (20) for uniform fields with directions between $b = [1\bar{1}0]$ (in-plane) and $c^* = [111]$ (out-of-plane). $\xi = 0$ corresponds to the hidden AFM Kitaev point $\widetilde{H}_K$ of Eq. (18), and $\xi = 1$ to the α-$RuCl_3$ model H_{RuCl}. The labels on the left axes show the energy scale of the Zeeman term as it enters Eq. (20). The labels on the right axes show the corresponding external field strengths $B = C\mu_B^{-1}|\mathbf{g}^{-1}\mathbf{h}|$ in tesla, when converting to the energy scale of α-$RuCl_3$ and assuming the anisotropic g tensor $\mathbf{g}$ of Ref. [64]. Phase boundaries are determined by peaks in $\partial_g^2 E_0$ and in χ_g. The quantum paramagnetic (QPM) phase is smoothly connected to the fully polarized state of the $h \to \infty$ limit. (a), (b) Field along $[1\bar{1}0]$, which corresponds to the crystallographic b axis of α-$RuCl_3$. (c), (d) $\mathbf{h}$ tilted from b towards $[111] = c^*$ by 30°. Assuming the mentioned g tensor, this corresponds to an external B-field tilted by ∼45°. (e), (f) $\mathbf{h} \parallel [111] = c^*$.

of mutually commuting local operators in the Kitaev model at zero field, we showed that dualities can be established between different field configurations and signs of the Kitaev coupling. Making use of these, we discuss the magnetic field-induced phases (including the novel phase Ψ_1) with the help of various (newly studied) correlators. For cases where the field does not directly couple to any of the classically degenerate spin configurations, we find the emergence of a field-induced *intermediate phase* (IP), related to previous studies of the AFM Kitaev model under a uniform field.

The existence of such an IP lying between the KSL and field-polarized states is deeply connected to the separation of energy scales between the Kitaev coupling K and the zero-field two-flux gap Δ_f at zero field. For fields incompatible with a classical ground state, K controls the scale at which the classical degeneracy is lifted. In contrast, Δ_f sets the stability of the low-field Kitaev spin liquid. Consistent with this picture, we found, on the one hand, that the IP is remarkably unstable towards field configurations that couple to a classical ground state, and, on the other hand, that for both the FM and AFM signs of the Kitaev interaction, the IP is stable for an extensive number of noncollinear fields related to one another via local duality transformations.

Interestingly, the locality of such dual transformations implies that fields inducing the IP need not be periodic with respect to translation. As a result, the momentum-space dynamical spin-structure factor—relevant for INS and ESR experiments—cannot represent a unique probe of the IP or related phase transitions. Instead, we studied the dynamical bond correlations—relevant for RIXS and Raman scattering measurements—and dynamical flux-flux correlations, which remain invariant under the dual transformations.

Independent of the field configuration, the field-induced phase transitions out of the KSL phase occur via proliferation of fluxes. However, we found that the suppression of the KSL occurs at sufficiently low fields that the dynamical timescale of the field-induced fluxes $\sim\hbar/\Delta_f$ remains large compared to the timescales associated with the matter fermion dynamics $\sim\hbar/K$. The separation of energy scales therefore also manifests as persistent plaquette operator correlations in phases adjacent to the KSL (including both the IP and asymptotically polarized phase). The observed correlations imply that a picture of effective couplings between slow dynamical fluxes mediated by the fast c-fermions may be applicable despite being outside the KSL.

Finally, to establish a relevance of the IP for real materials, we have studied models in the vicinity of a hidden Kitaev point, which hosts analogues of the AFM KSL and the field-induced IP under uniform fields. This point features large off-diagonal exchange couplings $\Gamma > 0$ and ferromagnetic Kitaev interactions $K < 0$ found in real materials. Surprisingly, we found that the IP extends in a large region of interaction parameter space and can be field-induced in models with zigzag order, including (J, K, Γ, J_3) models relevant for α-$RuCl_3$. For α-$RuCl_3$ our results predict that the IP is present for strong *out-of-plane* [111] fields. This establishes a connection between experimental studies of real materials and previous theoretical works on the IP. While we have focused our discussion on an α-$RuCl_3$-based model, the stability of the IP beyond the hidden Kitaev point may also extend to A_2IrO_3 ($A = \mathrm{Na}, \mathrm{Li}$) materials. We hope that this work motivates future studies probing such questions.

ACKNOWLEDGMENTS

We are grateful to R. Coldea, C. Hickey, S. Trebst, and J. G. Rau for stimulating discussions and acknowledge support by the Deutsche Forschungsgemeinschaft (DFG) through grant VA117/15-1. Computer time was allotted at the Centre for Scientific Computing (CSC) in Frankfurt.

APPENDIX A: SYMMETRIES AND DUALITIES AT ZERO AND FINITE FIELDS

In this Appendix, we review the construction of general symmetries of the Kitaev model. An important feature of the Kitaev Hamiltonian at zero field is the existence of a macroscopic number of mutually commuting Wilson loop operators $\{W_L\}$ that also commute with H_K. On a torus, any combination of loops $\{L\}$ can be constructed as products of plaquette operators $\{W_p\}$ and large loop operators running around the periodic boundaries, i.e., $W_L = W_{p_1} W_{p_2} \ldots W_{p_n}$. Together, such loop operators form the generators for *local* symmetry transformations $e^{\frac{i}{2}\alpha W_L} H_K e^{-\frac{i}{2}\alpha W_L} = H_K$ with $0 \leqslant \alpha < 2\pi$. For a Hamiltonian $H = H_K + H_1$, all perturbations ${H_1}' = e^{\frac{i}{2}\alpha W_L} H_{1K} e^{-\frac{i}{2}\alpha W_L}$ are formally equivalent to H_1 for all L and α. For our purpose, we focus on the specific case $\alpha = \pi$, for which spin operators $\mathcal{O} = S_i^\mu S_j^\nu S_k^\rho \ldots$ transform as $\mathcal{O}' = \pm\mathcal{O}$, depending on whether they commute $(+)$ or anticommute $(-)$ with W_L. The honeycomb lattice is thus divided into four sublattices, according to the transformation associated with each site:

$$W_L : (x', y', z') = \begin{cases} (x, y, z), & \text{sublattice A} \\ (x, -y, -z), & \text{sublattice B} \\ (-x, y, -z), & \text{sublattice C} \\ (-x, -y, z), & \text{sublattice D} \end{cases}. \tag{A1}$$

Transformations generated by specific loop operators W_L are shown in Figs. 12(a)–12(d). A specific example, shown in Fig. 12(d), is the "Klein" transformation employed in Refs. [57,63,74], which is associated to the operator W_{Klein} given by the product of plaquette operators on $\frac{1}{4}$ of the hexagonal plaquettes [Fig. 12(c)]. As noted above, the pure Kitaev Hamiltonian is mapped to itself by all such transformations, preserving the sign of the coupling ($K' = K$). However, the operators associated with a magnetic field generally do not commute with W_L. Let us consider a general field term described by

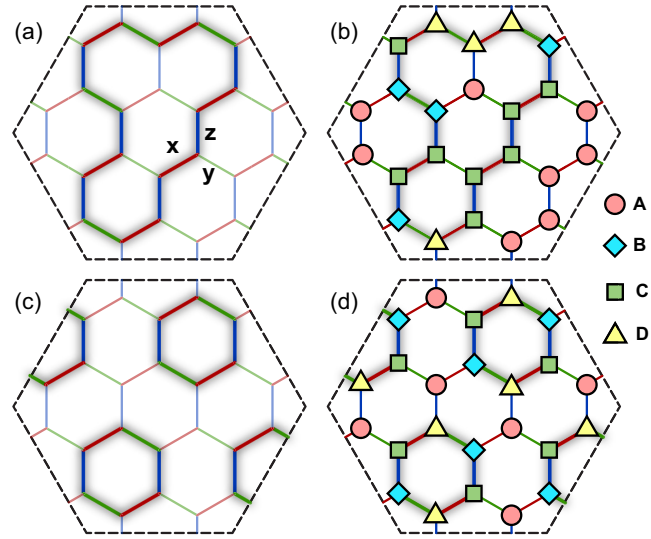

FIG. 12. Construction of general four-sublattice symmetry transformations for the Kitaev model with $\alpha = \pi$. (a) Example of a loop L. The associated operator W_L generates the symmetry transformation shown in (b). The specific operator W_{Klein} depicted in (c) leads to the "Klein" transformation (d) employed in Refs. [57,63,74].

$$H_{\mathrm{f}} = -\sum_i h_i^x S_i^x + h_i^y S_i^y + h_i^z S_i^z, \tag{A2}$$

where h_i^μ may take different values at each site. The equivalency of all combinations of local fields $W_L H_{\mathrm{f}} W_L$ generated by different L has several consequences.

In Sec. II, we discussed the appearance of the gapless IP in the AFM Kitaev model for uniform [111] fields $H_{\mathrm{f}} = H_{[111]}$, where $h_i^x = h_i^y = h_i^z = h$. By symmetry, equivalent states are also induced by all nonuniform field configurations described by $W_L H_{[111]} W_L$. For all such fields, the product of γ components of the local fields on a γ bond is positive, i.e. $h_i^\gamma h_j^\gamma > 0$. Since all IP states appearing for $H = H_K + W_L H_{[111]} W_L$ are smoothly connected by continuous unitary transformations, they belong to a common intermediate-field phase. However these transformations do not commute with the spin operators, so that the dynamical spin-structure factor $\mathcal{S}(\mathbf{k}, \omega)$ does not provide a unique characterization of the common IP. In contrast, $S_i^\gamma S_j^\gamma$ and W_p commute with all W_L, and therefore $\mathcal{I}_X(\mathbf{k}, \omega)$ and $\mathcal{W}(\mathbf{k}, \omega)$ reflect more intrinsic characteristics that are common across all equivalent IP states.

A similar approach can be used to establish correspondence between the FM and AFM Kitaev models. We define P_3, which permutes the spin components $(x, y, z) \to (y, z, x)$ on every site. Combining this with the operator W_{Klein} [see Fig. 12(c)] leads to $\mathcal{G} \equiv e^{\frac{i}{2}\pi P_3^{-1} W_{\mathrm{Klein}} P_3}$, that commutes with all W_p, but anticommutes with all bond operators $S_i^\gamma S_j^\gamma$. As a result, $\mathcal{G} H_K \mathcal{G}^{-1} = -H_K$, providing a duality transformation that relates the AFM and FM Kitaev models at zero field (i.e.,

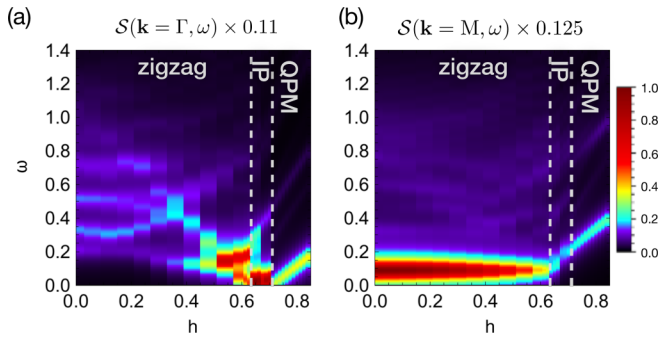

FIG. 13. Dynamical spin-structure factor of $H(\xi = 1, h)$ [Eq. (20)] under a [111] field. Poles obtained via ED were broadened by 0.05.

$K' = -K$). The transformation in real space is

$$\mathcal{G} : (x', y', z') = \begin{cases} (x, y, z), & \text{sublattice A} \\ (-x, y, -z), & \text{sublattice B} \\ (-x, -y, z), & \text{sublattice C} \\ (x, -y, -z), & \text{sublattice D} \end{cases} \tag{A3}$$

with the sublattice pattern shown in Fig. 12(d). Under the transformation $\mathcal{G}$, a uniform [111] field $H_{[111]}$ becomes a four-sublattice "tetrahedral" field $\mathcal{G}H_{[111]}\mathcal{G}^{-1}$, with local fields $\mathbf{h}_i$ oriented along the [111], $[\bar{1}1\bar{1}]$, $[1\bar{1}\bar{1}]$, or $[\bar{1}\bar{1}1]$ directions as shown in Fig. 8.

If this tetrahedral field is applied to the AFM Kitaev model, it acts as a uniform field in the FM model; the tetrahedral field directly couples to one of the classically degenerate states and opens a gap immediately after the suppression of the KSL. Conversely, if the tetrahedral field is applied to the FM Kitaev model, it acts as a uniform field in the AFM model, yielding a gapless intermediate phase. This IP in the FM Kitaev model is continuously connected to the IP of the AFM Kitaev model via the unitary transformation $\mathcal{G}$, and therefore represents the same phase. For field configurations that are dual to one another, the FM model displays precisely identical dynamical flux-flux and bond-bond correlations to those observed in the AFM model. This follows from the fact that $\mathcal{G}$ commutes with W_p and anticommutes with $S_i^\gamma S_j^\gamma$.

APPENDIX B: DYNAMICAL SPIN-STRUCTURE FACTOR OF H_{RuCl} UNDER A [111] FIELD

In Fig. 13, we show the DSSF of $H(\xi = 1, h)$ [Eq. (20)] under a [111] field, which corresponds to the H_{RuCl} model of Eq. (19). At zero field, the response shows sharp low-energy single-magnon excitations at $\mathbf{q} = \mathrm{M}$, and a broad scattering continuum at $\mathbf{q} = \Gamma$ [65]. Upon applying the [111] field, the $\mathbf{q} = \mathrm{M}$ magnon does not shift in energy, but it looses significant intensity upon increasing the field towards h_{c1}. At $\mathbf{q} = \Gamma$, the broad range of excitations at zero field narrows upon increasing h, with large amounts of spectral weight shifting to lower energies. In the IP at $h_{c1} < h < h_{c2}$, the DSSF shows most spectral weight at $\mathbf{q} = \Gamma$ and energies $\omega \lesssim 0.8$ meV, originating from a highly increased low-energy density of states in the IP, that extends down to lowest energies near $\omega \sim 0$. These excitations show no distinct field-dependence within the IP region, which is in sharp contrast to the excitations in the QPM at $h > h_{c2}$. The low-energy $\mathbf{q} = \Gamma$ excitation in the QPM shows a linear field dependence with slope $\mathrm{d}\omega/\mathrm{d}h \approx \Delta S = 1$ as expected for a single magnon in the asymptotically polarized QPM state.

[1] A. Kitaev, Ann. Phys. **321**, 2 (2006).
[2] G. Jackeli and G. Khaliullin, Phys. Rev. Lett. **102**, 017205 (2009).
[3] Y. Cui, J. Zheng, K. Ran, J. Wen, Z.-X. Liu, B. Liu, W. Guo, and W. Yu, Phys. Rev. B **96**, 205147 (2017).
[4] T. Biesner, S. Biswas, W. Li, Y. Saito, A. Pustogow, M. Altmeyer, A. U. B. Wolter, B. Büchner, M. Roslova, T. Doert, S. M. Winter, R. Valentí, and M. Dressel, Phys. Rev. B **97**, 220401(R) (2018).
[5] G. Bastien, G. Garbarino, R. Yadav, F. J. Martinez-Casado, R. Beltrán Rodríguez, Q. Stahl, M. Kusch, S. P. Limandri, R. Ray, P. Lampen-Kelley, D. G. Mandrus, S. E. Nagler, M. Roslova, A. Isaeva, T. Doert, L. Hozoi, A. U. B. Wolter, B. Büchner, J. Geck, and J. van den Brink, Phys. Rev. B **97**, 241108(R) (2018).
[6] Z. Wang, J. Guo, F. F. Tafti, A. Hegg, S. Sen, V. A. Sidorov, L. Wang, S. Cai, W. Yi, Y. Zhou, H. Wang, S. Zhang, K. Yang, A. Li, X. Li, Y. Li, J. Liu, Y. Shi, W. Ku, Q. Wu, R. J. Cava, and L. Sun, Phys. Rev. B **97**, 245149 (2018).
[7] L. J. Sandilands, Y. Tian, K. W. Plumb, Y.-J. Kim, and K. S. Burch, Phys. Rev. Lett. **114**, 147201 (2015).
[8] J. Nasu, J. Knolle, D. L. Kovrizhin, Y. Motome, and R. Moessner, Nat. Phys. **12**, 912 (2016).
[9] S.-H. Do, S.-Y. Park, J. Yoshitake, J. Nasu, Y. Motome, Y. S. Kwon, D. T. Adroja, D. J. Voneshen, K. Kim, T. H. Jang, J. H. Park, K.-Y. Choi, and S. Ji, Nat. Phys. **13**, 1079 (2017).
[10] R. D. Johnson, S. C. Williams, A. A. Haghighirad, J. Singleton, V. Zapf, P. Manuel, I. I. Mazin, Y. Li, H. O. Jeschke, R. Valentí, and R. Coldea, Phys. Rev. B **92**, 235119 (2015).
[11] R. Yadav, N. A. Bogdanov, V. M. Katukuri, S. Nishimoto, J. van den Brink, and L. Hozoi, Sci. Rep. **6**, 37925 (2016).
[12] J. A. Sears, Y. Zhao, Z. Xu, J. W. Lynn, and Y.-J. Kim, Phys. Rev. B **95**, 180411(R) (2017).
[13] A. U. B. Wolter, L. T. Corredor, L. Janssen, K. Nenkov, S. Schönecker, S.-H. Do, K.-Y. Choi, R. Albrecht, J. Hunger, T. Doert, M. Vojta, and B. Büchner, Phys. Rev. B **96**, 041405(R) (2017).
[14] S.-H. Baek, S.-H. Do, K.-Y. Choi, Y. S. Kwon, A. U. B. Wolter, S. Nishimoto, J. van den Brink, and B. Büchner, Phys. Rev. Lett. **119**, 037201 (2017).
[15] Z. Wang, S. Reschke, D. Hüvonen, S.-H. Do, K.-Y. Choi, M. Gensch, U. Nagel, T. Rõõm, and A. Loidl, Phys. Rev. Lett. **119**, 227202 (2017).
[16] J. Zheng, K. Ran, T. Li, J. Wang, P. Wang, B. Liu, Z.-X. Liu, B. Normand, J. Wen, and W. Yu, Phys. Rev. Lett. **119**, 227208 (2017).

[17] A. N. Ponomaryov, E. Schulze, J. Wosnitza, P. Lampen-Kelley, A. Banerjee, J.-Q. Yan, C. A. Bridges, D. G. Mandrus, S. E. Nagler, A. K. Kolezhuk, and S. A. Zvyagin, Phys. Rev. B **96**, 241107(R) (2017).

[18] A. Banerjee, P. Lampen-Kelley, J. Knolle, C. Balz, A. A. Aczel, B. Winn, Y. Liu, D. Pajerowski, J. Yan, C. A. Bridges, A. T. Savici, B. C. Chakoumakos, M. D. Lumsden, D. A. Tennant, R. Moessner, D. G. Mandrus, and S. E. Nagler, npj Quantum Mater. **3**, 8 (2018).

[19] R. Hentrich, A. U. B. Wolter, X. Zotos, W. Brenig, D. Nowak, A. Isaeva, T. Doert, A. Banerjee, P. Lampen-Kelley, D. G. Mandrus, S. E. Nagler, J. Sears, Y.-J. Kim, B. Büchner, and C. Hess, Phys. Rev. Lett. **120**, 117204 (2018).

[20] Y. Kasahara, T. Ohnishi, Y. Mizukami, O. Tanaka, S. Ma, K. Sugii, N. Kurita, H. Tanaka, J. Nasu, Y. Motome, T. Shibauchi, and Y. Matsuda, Nature (London) **559**, 227 (2018).

[21] L. Janssen and M. Vojta, J. Phys.: Condens. Matter **31**, 423002 (2019).

[22] Z. Zhu, I. Kimchi, D. N. Sheng, and L. Fu, Phys. Rev. B **97**, 241110(R) (2018).

[23] M. Gohlke, R. Moessner, and F. Pollmann, Phys. Rev. B **98**, 014418 (2018).

[24] H.-C. Jiang, C.-Y. Wang, B. Huang, and Y.-M. Lu, arXiv:1809.08247.

[25] L. Zou and Y.-C. He, arXiv:1809.09091.

[26] N. D. Patel and N. Trivedi, Proc. Natl. Acad. Sci. USA **116**, 12199 (2019).

[27] C. Hickey and S. Trebst, Nat. Commun. **10**, 530 (2019).

[28] M.-H. Jiang, S. Liang, W. Chen, Y. Qi, J.-X. Li, and Q.-H. Wang, arXiv:1903.01279.

[29] G. Baskaran, D. Sen, and R. Shankar, Phys. Rev. B **78**, 115116 (2008).

[30] G. Baskaran, S. Mandal, and R. Shankar, Phys. Rev. Lett. **98**, 247201 (2007).

[31] J. Knolle, D. L. Kovrizhin, J. T. Chalker, and R. Moessner, Phys. Rev. Lett. **112**, 207203 (2014).

[32] J. Knolle, D. L. Kovrizhin, J. T. Chalker, and R. Moessner, Phys. Rev. B **92**, 115127(R) (2015).

[33] G. B. Halász, N. B. Perkins, and J. van den Brink, Phys. Rev. Lett. **117**, 127203 (2016).

[34] J. Knolle, G.-W. Chern, D. L. Kovrizhin, R. Moessner, and N. B. Perkins, Phys. Rev. Lett. **113**, 187201 (2014).

[35] X.-Y. Song, Y.-Z. You, and L. Balents, Phys. Rev. Lett. **117**, 037209 (2016).

[36] H.-C. Jiang, Z.-C. Gu, X.-L. Qi, and S. Trebst, Phys. Rev. B **83**, 245104 (2011).

[37] S. Liang, M.-H. Jiang, W. Chen, J.-X. Li, and Q.-H. Wang, Phys. Rev. B **98**, 054433 (2018).

[38] J. Nasu, Y. Kato, Y. Kamiya, and Y. Motome, Phys. Rev. B **98**, 060416(R) (2018).

[39] L. Janssen, E. C. Andrade, and M. Vojta, Phys. Rev. Lett. **117**, 277202 (2016).

[40] P. A. McClarty, X.-Y. Dong, M. Gohlke, J. G. Rau, F. Pollmann, R. Moessner, and K. Penc, Phys. Rev. B **98**, 060404(R) (2018).

[41] For a classical product state with collinear spins (such as the fully polarized state), the flux density is constrained to be close to 0.5, with $\frac{13}{27} \leqslant \langle n_p \rangle \leqslant \frac{14}{27}$. Noncollinear classical states are less constrained, and may have $\frac{1}{3} \leqslant \langle n_p \rangle \leqslant \frac{2}{3}$.

[42] V. Lahtinen, New J. Phys. **13**, 075009 (2011).

[43] V. Lahtinen, A. W. W. Ludwig, J. K. Pachos, and S. Trebst, Phys. Rev. B **86**, 075115(R) (2012).

[44] V. Lahtinen, A. W. W. Ludwig, and S. Trebst, Phys. Rev. B **89**, 085121 (2014).

[45] H. Théveniaut and M. Vojta, Phys. Rev. B **96**, 054401 (2017).

[46] S.-S. Zhang, Z. Wang, G. B. Halász, and C. D. Batista, Phys. Rev. Lett. **123**, 057201 (2019).

[47] On the high-symmetry 24-site cluster under uniform [111]-fields, $\partial_h^2 E_0$ and χ_h show multiple anomalies within the IP region, reflecting level crossings between nearly degenerate discrete states. However, these level crossing occur without qualitative changes in any static or dynamic observable. Previous studies have mitigated such effects by (i) employing clusters that do not respect C_3 symmetry [22–26,72], (ii) rotating **h** slightly away from [111] [27], or (iii) introducing different coupling strengths on different bond types.

[48] D. Gotfryd, J. Rusnačko, K. Wohlfeld, G. Jackeli, J. Chaloupka, and A. M. Oleś, Phys. Rev. B **95**, 024426 (2017).

[49] J. G. Rau, E. K.-H. Lee, and H.-Y. Kee, Phys. Rev. Lett. **112**, 077204(R) (2014).

[50] S. M. Winter, Y. Li, H. O. Jeschke, and R. Valentí, Phys. Rev. B **93**, 214431 (2016).

[51] V. M. Katukuri, S. Nishimoto, V. Yushankhai, A. Stoyanova, H. Kandpal, S. Choi, R. Coldea, I. Rousochatzakis, L. Hozoi, and J. van den Brink, New J. Phys. **16**, 013056 (2014).

[52] Y. Yamaji, Y. Nomura, M. Kurita, R. Arita, and M. Imada, Phys. Rev. Lett. **113**, 107201 (2014).

[53] H.-S. Kim and H.-Y. Kee, Phys. Rev. B **93**, 155143 (2016).

[54] W. Wang, Z.-Y. Dong, S.-L. Yu, and J.-X. Li, Phys. Rev. B **96**, 115103 (2017).

[55] S. M. Winter, A. A. Tsirlin, M. Daghofer, J. van den Brink, Y. Singh, P. Gegenwart, and R. Valentí, J. Phys.: Condens. Matter **29**, 493002 (2017).

[56] R. Yadav, S. Rachel, L. Hozoi, J. van den Brink, and G. Jackeli, Phys. Rev. B **98**, 121107(R) (2018).

[57] J. Chaloupka and G. Khaliullin, Phys. Rev. B **92**, 024413 (2015).

[58] J. Chaloupka and G. Khaliullin, Phys. Rev. B **94**, 064435 (2016).

[59] A. Koitzsch, E. Mueller, M. Knupfer, B. Buechner, D. Nowak, A. Isaeva, T. Doert, M. Grueninger, S. Nishimoto, and J. van den Brink, arXiv:1709.02712.

[60] I. Yamauchi, M. Hiraishi, H. Okabe, S. Takeshita, A. Koda, K. M. Kojima, R. Kadono, and H. Tanaka, Phys. Rev. B **97**, 134410 (2018).

[61] J. Cookmeyer and J. E. Moore, Phys. Rev. B **98**, 060412(R) (2018).

[62] S. D. Das, S. Kundu, Z. Zhu, E. Mun, R. D. McDonald, G. Li, L. Balicas, A. McCollam, G. Cao, J. G. Rau, H.-Y. Kee, V. Tripathi, and S. E. Sebastian, Phys. Rev. B **99**, 081101(R) (2019).

[63] J. Chaloupka, G. Jackeli, and G. Khaliullin, Phys. Rev. Lett. **105**, 027204 (2010).

[64] S. M. Winter, K. Riedl, D. Kaib, R. Coldea, and R. Valentí, Phys. Rev. Lett. **120**, 077203 (2018).

[65] S. M. Winter, K. Riedl, P. A. Maksimov, A. L. Chernyshev, A. Honecker, and R. Valentí, Nat. Commun. **8**, 1152 (2017).

[66] K. Riedl, Y. Li, S. M. Winter, and R. Valentí, Phys. Rev. Lett. **122**, 197202 (2019).

[67] The studies of Refs. [61,68,69] found further measurements well reproduced by the model with slightly adjusted parameters.

[68] P. Lampen-Kelley, L. Janssen, E. C. Andrade, S. Rachel, J.-Q. Yan, C. Balz, D. G. Mandrus, S. E. Nagler, and M. Vojta, arXiv:1807.06192.

[69] L. Wu, A. Little, E. E. Aldape, D. Rees, E. Thewalt, P. Lampen-Kelley, A. Banerjee, C. A. Bridges, J.-Q. Yan, D. Boone, S. Patankar, D. Goldhaber-Gordon, D. Mandrus, S. E. Nagler, E. Altman, and J. Orenstein, Phys. Rev. B **98**, 094425 (2018).

[70] J. S. Gordon, A. Catuneanu, E. S. Sørensen, and H.-Y. Kee, Nat. Commun. **10**, 2470 (2019).

[71] The magnetic torque response of H_{RuCl} is found to be nearly unaffected by the presence of the IP on sweeping the field angle, and was thus not discussed in the study of Ref. [66] on the same model.

[72] Y.-F. Jiang, T. P. Devereaux, and H.-C. Jiang, Phys. Rev. B **100**, 165123 (2019).

[73] L. Janssen, E. C. Andrade, and M. Vojta, Phys. Rev. B **96**, 064430 (2017).

[74] J. Chaloupka, G. Jackeli, and G. Khaliullin, Phys. Rev. Lett. **110**, 097204 (2013).